CHAPTER 1

INTRODUCTION

The Lao Pako archaeological site locates on a hill at the southern bank of Nam Ngum River, in Phonkham village, Pak Ngum district, Vientiane Capital, Lao PDR (Figure 1.1). The exact position of the Lao Pako archaeological site is longitude $102^{o}51'28.038''$ *E* and latitude $18^{o}09'29.904''$ *N* (Figure 1.2). It was a place where people came to work with iron and buried groups of ceramic vessels during the 4^{th} to 6^{th} centuries AD.

There are many artifacts found in Lao Pako. This is a very important evidence to prove that people used to live here in the past. It has been known as tourism resort since 2002. Lao Pako is an interesting place for archaeological study. Archaeological investigations were carried out during 1994 to 2003. In 1994, one trench was excavated by Lao archaeologists. Under the Lao-Swedish Joint Research Project, the archaeological excavations were conducted in three periods. In 1995, three trenches were excavated. In 2000, sites close to Lao Pako were investigated. In 2002-2003, 16 test pits had been excavated. Many potteries and metal product materials were found in the excavation. Three charcoal samples from excavation in 1995 had been dated with the ^{14}C dating method. The result shows that its cultural layer was approximately between 350 and 600 AD. There are artifacual and structural relation between Lao Pako and archaeological sites such as Ban Chieng, Ban Na Di, Noen-U-Lok and Ban Kan Luang on the south of Korat Plateau, North-East of Thailand.

Archaeological sites provide valuable information for countries. In addition, buried archaeological remains in Lao Pako, such as ceramic and metallic objects, possess different physical properties from surrounding ground. Moreover, the properties of soil disturbed by human activities in the past such as digging for burying some things may be different from primary soil due to its density, moistures, etc. Geophysical methods are considered to be useful for archaeological works in determining

structure, location and feature of the buried archaeological objects. The geophysical methods are a non-destructive technique and spend shorter time for measurement. Therefore, application of geophysical methods has been widely and successfully applied for archaeological investigation such as ground penetrating radar method (Vaughan, 1986; Goodman, 1994; Imai, 1987; Hruska et al., 1999; Brasile et al., 2000; Gracia et al., 2000; Cezar et al., 2001; Leucci et al., 2006; Quarto et al., 2007), magnetic methods (Gibson, 1986; Hamiton, 1984; Jeng et al., 2003; Büyüksaraç et al.,2006), and resistivity method (Tsokas and Toulors, 1997; Kai et al., 2004). The combination of geophysical methods also employed in archaeological investigation in order to obtain better resolutions ; for example; integration of magnetic, resistivity and ground penetrating radar investigations (Sambuelli et al., 1999 and Drahor et al., 2006), application of magnetic and resistivity methods (Aitken, 1961; Gibson, 1986; Hesse et al., 1986; Scollar et., al 1986; Young and Droege,1986; Casas et al., 1989), and GPR and resistivity (Ima et al.,1978; Vafidis et al., 2005, and Negri et al., 2006).

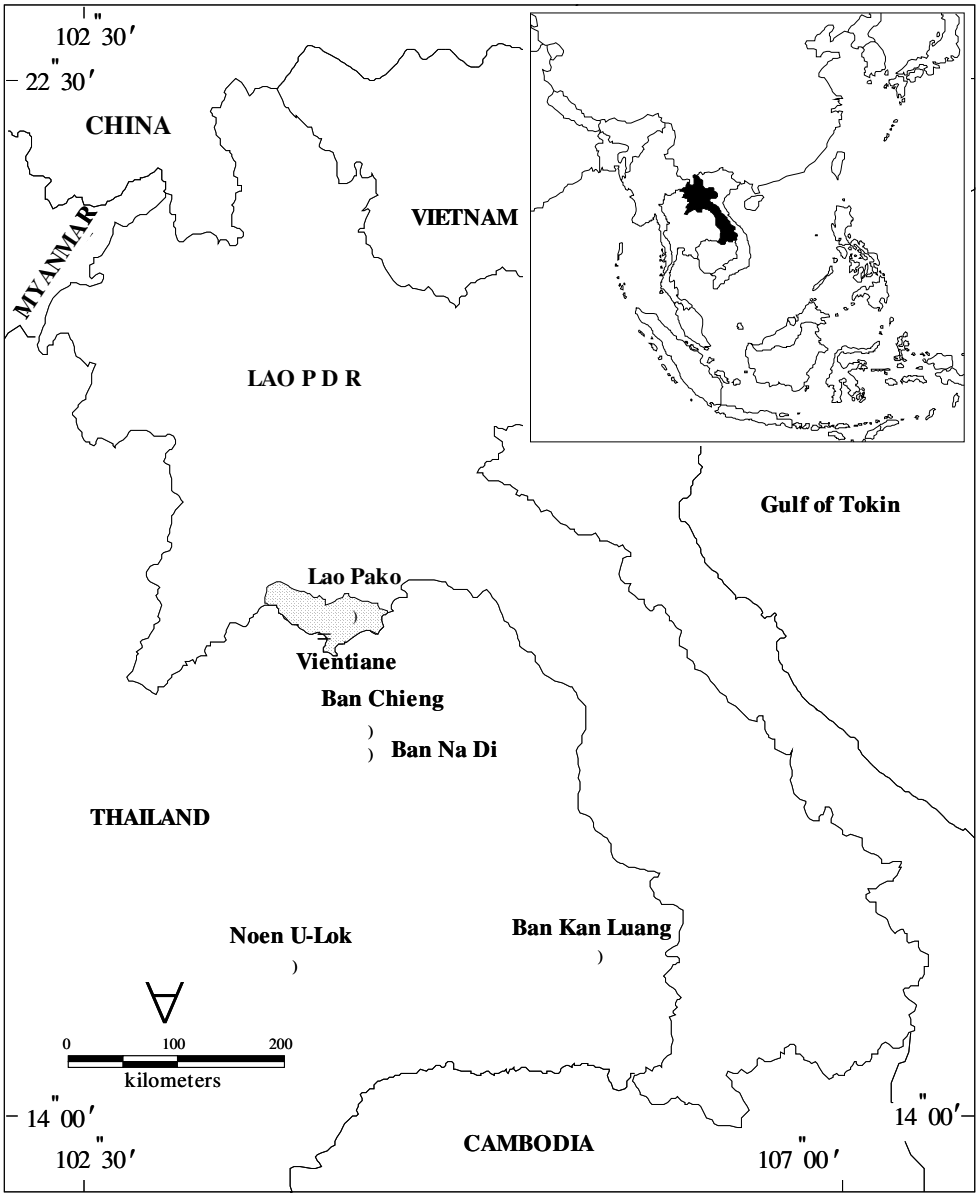

Figure 1.1 The map of Lao PDR and location of study area.

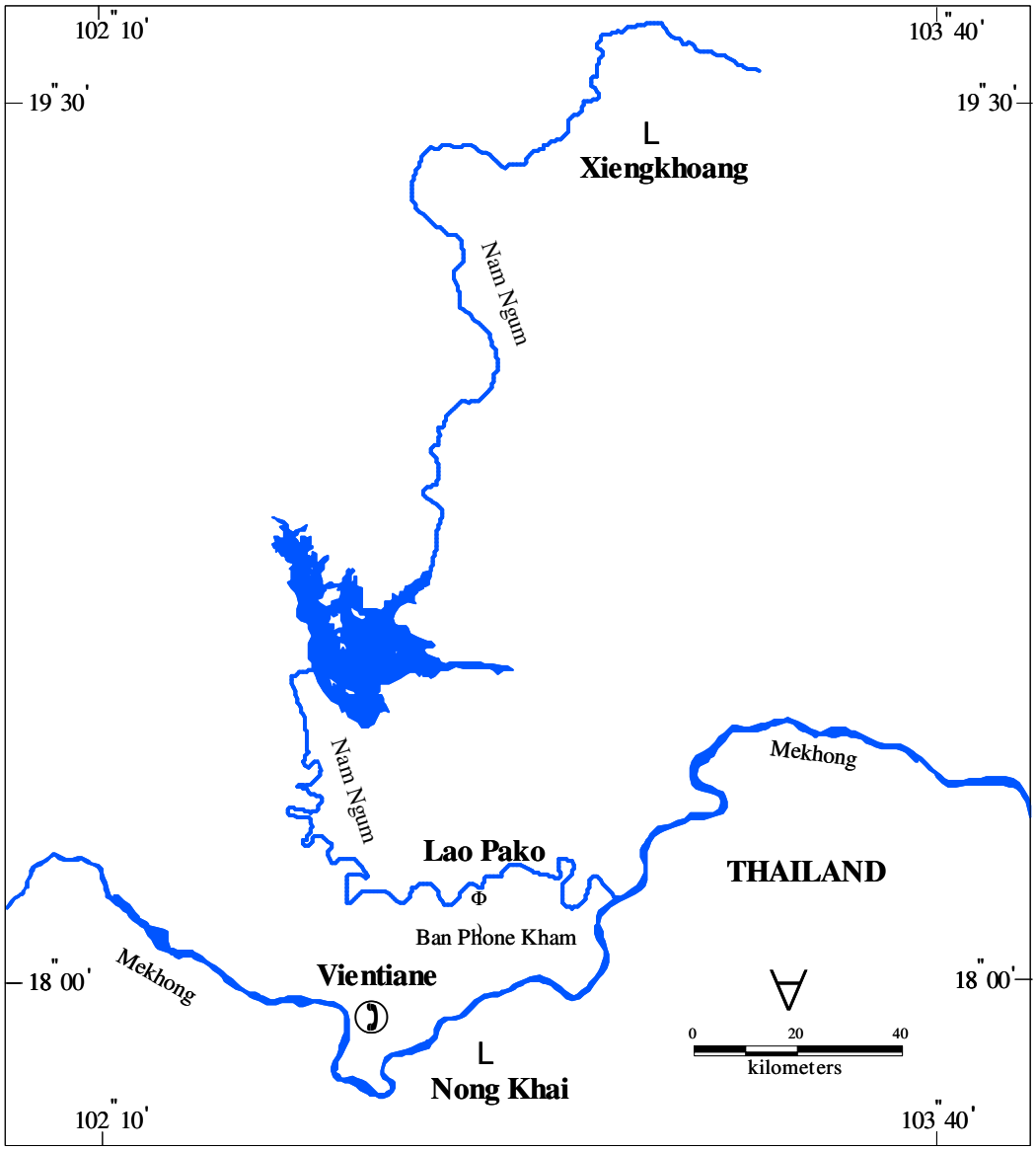

Figure 1.2 The location of study area, Lao Pako archaeological site.

1.1 Theory of geophysical methods

Geophysical methods used for investigating the shallow feature of the earth's crust vary in accordance with the physical properties of rocks. For example when there is a contrast in magnetic susceptibility in the ground, magnetic method can be conducted to determine location and depth of the objects. Similarly, in case of electric conductivity, the electrical or electromagnetic methods will be chosen for the investigation. In archaeological problem, the physical properties of buried archaeological objects may probably be different from surrounding soil. Hence in this work, the geophysical methods were employed to map soil layers and locate disturbances in subsurface relating to archaeological features. There are four different geophysical methods carried out in this study; magnetic mapping, ground penetrating radar, resistivity mapping and continuous vertical electrical sounding. The concepts of each the methods are explained as followings;

1.1.1 Ground penetrating radar

1.1.1.1 Concepts

Ground penetrating radar (GPR) employs the propagation of high-frequency (10 MHz-1000 MHz) electromagnetic pulse. The radar pulse emitted by an antenna is transmitted into the ground. When it reaches an interface of ground where there is a change in electric and magnetic property, pulse will reflect and refract. The reflected pulses return to the receiving antenna, and the arrival two-way time is measured. The position of reflector can be determined when the velocity of the pulse is known (Figure 1.3(a)). The methodology employed in reflected seismic method, such as data acquisition, processing, and displaying, can be applied for GPR measurement. In contrast to seismic methods, GPR uses electromagnetic waves instead of acoustic waves.

In general, the electromagnetic waves are not penetrating as deep as acoustic waves but it can map subsurface features with high resolution. An example of radar section is shown in Figure 1.3(b).

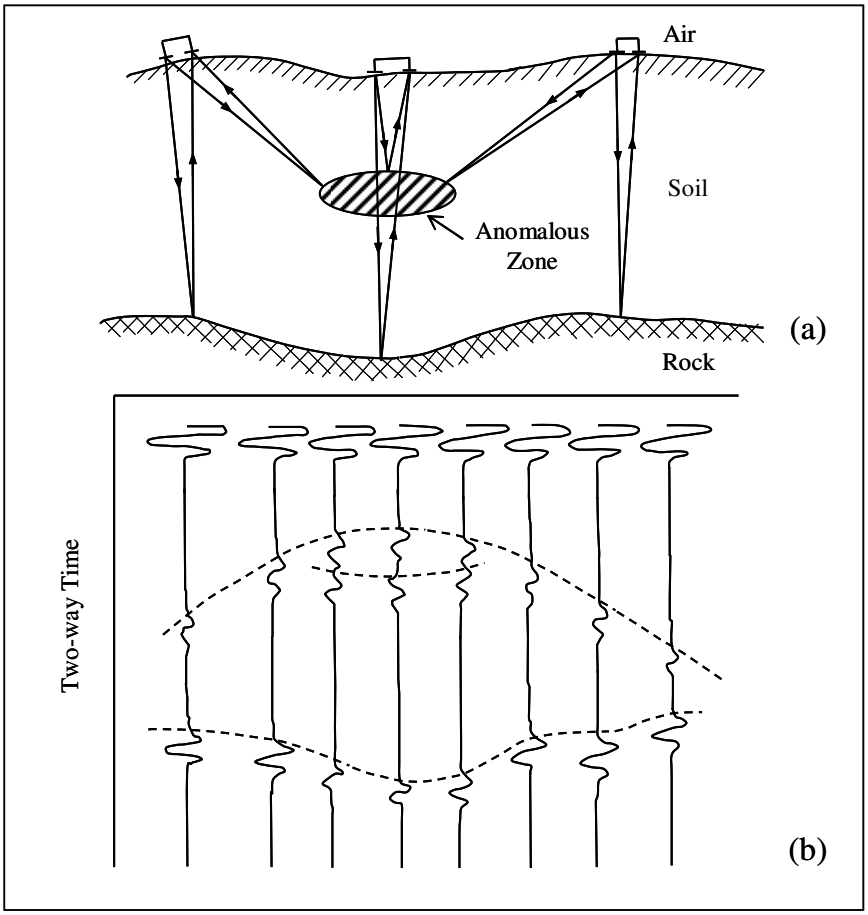

Figure 1.3 (a) Conceptual illustration of GPR used in the reflection profile mode on soil over bedrock and (b) Radar record obtained over the idealized situation in (a) (Modified from Davis and Annan, 1989).

2.1.1.2 Electromagnetic propagation parameter and electrical properties

The velocity and the attenuation are the factors that describe the propagation of electromagnetic wave. The parameters, determining how efficiently the wave propagates into medium, are the dielectric and conductivity properties of the material. This can be described by the following equation:

$$\nabla^2 E + \omega^2 \mu\sigma E + i\omega\mu\varepsilon = 0 \qquad (1.1)$$

E is the electric field (V/m); σ is the conductivity (S/m), ε is the electrical permittivity of material ($\varepsilon = \varepsilon_0 \varepsilon_r$, F/m) , ε_0 is the electrical permittivity of free space (8.854×10^{-12} F/m), ε_r is the relative dielectric permittivity of the material, μ is the magnetic permeability of the material (H/m), ω is the angular frequency , $2\pi f$ (rad/s), $i = \sqrt{-1}$, and t is the time (s). From equation (1.1), the expression involves energy losing of electromagnetic wave and we assume that μ, σ and ε_0 for homogenous material are the followings;

$$E = E_0 e^{i(kz - \omega t)} \tag{1.2}$$

Where $k = \left(\omega^2 \varepsilon\mu + i\omega\sigma\right)^{1/2} = \alpha + i\beta$ and $\delta = \frac{1}{\rho}$

k is the propagation parameter or wave number. The real and imaginary part of wave number can be expressed as follows

$$\alpha = \omega \left\{ \frac{\varepsilon\mu}{2} \left[\sqrt{1 + \frac{\sigma}{\omega^2 \varepsilon^2}} + 1 \right] \right\}^{1/2} \tag{1.3}$$

$$\beta = \omega \left\{ \frac{\varepsilon\mu}{2} \left[\sqrt{1 + \frac{\sigma}{\omega^2 \varepsilon^2}} - 1 \right] \right\}^{1/2} \tag{1.4}$$

In a low loss-medium, attenuation is usefully expressed as (Davis and Annan, 1989).

$$\alpha = \frac{1.69 \times 10^3 \sigma}{\sqrt{\varepsilon}} \tag{1.5}$$

1.1.1.3 Q and loss tangent

The parameter that determines how efficiently an electromagnetic wave propagated in a medium is $\rho\varepsilon\omega$, often denoted by Q, also written as $\varepsilon\omega/\sigma$.The inverse $1/Q = \sigma/\omega\varepsilon$ is called the loss tangent. If $Q >> 1$, the wave will propagate efficiently without appreciable loss of energy over large distance. In contrast, If $Q < 1$, the wave is attenuated with in a short distance (Parasnis, 1998).

1.1.1.4 Skin depth

The attenuation of the EM wave, reducing of amplitude of the field with distance, is expressed in term of the "skin depth", Z or depth of the wave penetration.

$$Z = \frac{2}{\sigma}\sqrt{\frac{\varepsilon}{\mu}} \tag{1.6}$$

The depth of penetrating of radio waves depends on their frequency and the nature of the material being surveyed. Water content and porosity are important factor to control on penetration of electromagnetic wave. Moreover, in mediums with low resistivity such as clays or saltwater, the skin depth is in order of 15 cm. In contrast, when the wave travel in high resistive medium, for example dry sand, the skin depth is greater than 10 m. The attenuation only depends on the dielectric permittivity (ε) and electrical conductivity (σ) for frequency of megahertz range (10 MHz-1000 MHz) (Kearey et al., 2002).

1.1.1.5 Velocity of EM wave

In general, radar velocity depends on frequency, *dielectric constant (relative permittivity)* and conductivity wave of the subsurface. In practice, the velocity remains constant between 10 and 1000 MHz when GPR systems is operated at conductivity of less than 100 mS/s, $\sigma^2 / \omega^2 \varepsilon^2 << 1$. The velocity increases at frequencies greater than 1000 MHz due to the relaxation of water molecule. Normally, GPR system operates in the frequency range between 10 and 1000 MHz. Therefore, the velocity is constant and signal is not dispersed by frequency-dependent velocity. The radar velocities are only controlled by the *dielectric constant (relative dielectric permittivity)* and conductivities of the subsurface. The velocity of radar wave *(v)* is given by:

$$v = \frac{c}{\sqrt{(\mu_r \varepsilon_r)}} \tag{1.7}$$

Where c is the velocity of light in free space ($3x10^8 ms^{-1}$), μ_r is the relative magnetic permeability, and ε_r is the relative dielectric permittivity of medium.

Table 1.1 Typical dielectric constant, electrical conductivity, velocity and attenuation observed in common geological materials at 100 MHz (Davis and Annan, 1989).

Material	ε_r	σ (mS/m)	v (m/ns)	α (dB/m)
Air	1	0	0.30	0
Distilled water	80	0.01	0.033	0.002
Fresh water	80	0.5	0.033	0.1
Dry sand	3-5	0.01	0.15	0.01
Saturated sand	20-30	0.1-1.0	0.06	0.03-0.3
Shales	5-15	1-100	0.09	1-100
Silt	5-30	1-100	0.09	1-100
Clays	5-40	2-1000	0.06	1-300

1.1.1.6 Reflection and transmission

When of electromagnetic wave reaches interface between two media of different impedances, it is partly reflected and transmitted. The frequency of the electromagnetic wave is also constant. If we consider only non-magnetic media, $\mu_2 = \mu_1 = \mu_0$, the reflection coefficient, R can be expressed as

$$R = \frac{\sqrt{\varepsilon_{r2}} - \sqrt{\varepsilon_{r1}}}{\sqrt{\varepsilon_{r2}} + \sqrt{\varepsilon_{r1}}} = \frac{(v_2 - v_1)}{(v_2 + v_1)} \tag{1.8}$$

Where ε_{r1} and ε_{r2} are the relative dielectric permittivity of two media separated by the interface, and v_1 and v_2 are the velocity of EM wave within them. Velocities of EM wave within geological materials generally range between 0.06 and 0.175 m ns^{-1}.

1.1.1.7 Velocity estimation

The propagation velocity of EM wave in a medium can be determined by analysis of point source hyperbolas appearing in the radar section. The hyperbolic pattern results from diffraction of EM wave when it reach small object in the medium. Velocity of EM wave can be determined from the hyperbolic parameters as follow.

$$v_{RMS} = \sqrt{\frac{x_2^2 - x_1^2}{t_2^2 - t_1^2}} \tag{1.9}$$

Where x_1 and x_2 are the positions along of mid point of antenna.

t_1 and t_2 are two way time hyperbolic branch at x_1 and x_2 respectively.

v_{RMS} is an average velocity of EM wave in the medium from the surface to the diffraction point.

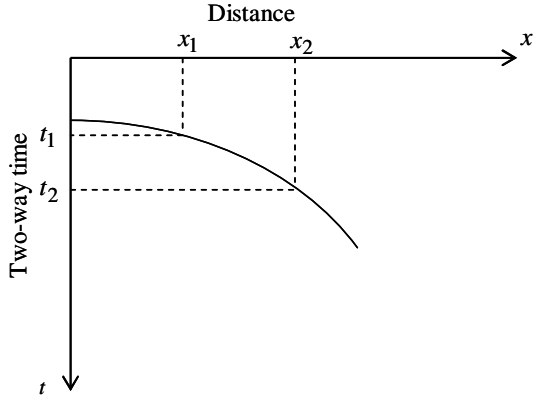

Figure 1.4 The two way time-distance curve of reflected EM wave.

1.1.1.8 Depth determination

The depth (h) to the reflector (Figure 1.5) can be calculated from

$$h = \frac{\left(v^2 t^2 - x^2\right)^{1/2}}{2} \tag{1.10}$$

Where v is the velocity of EM wave in the medium.

t is the two way time for the pulse to go to the reflector and return to the antenna.

h is the depth to the reflector.

x is the distance between transmitter and receiver.

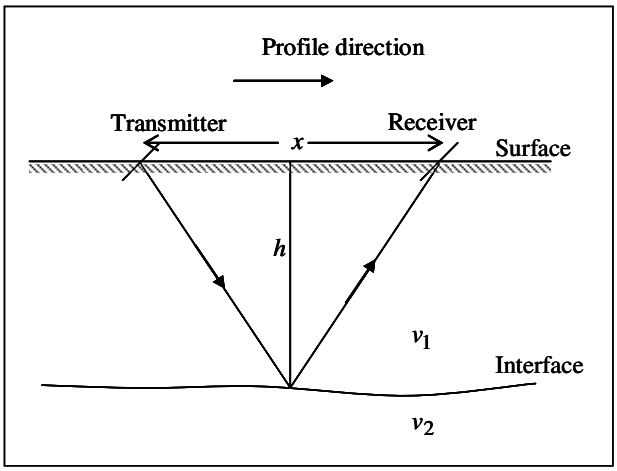

Figure 1.5 GPR configuration.

1.1.1.9 The GPR system

GPR system comprises four main parts; the transmitting unit, the receiving unit, control unit and the display unit. A simple diagram of a GPR system is shown in Figure 1.6. The transmitter generates and sends electromagnetic pulse into the ground. The reflected signal is detected by receiving antenna. Then the signal data is sent to the control unit and the displayed radargram, amplitude of the reflected pulses at different arrival.

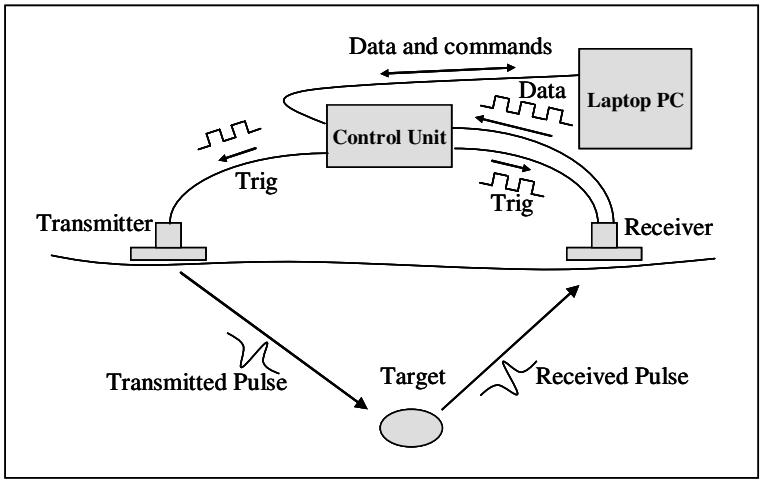

Figure 1.6 Schematic diagram of the GPR system.

1.1.2 Magnetic Method

1.1.2.1 Basic concept of geomagnetism

Magnetic flux exists around the magnet, as indicated by the flux lines flows from one end of magnet to another and converges near the ends of the magnet (Figure 1.7). The points within the magnet where the flux converge are known as the magnetic poles.

The force F between two magnetic poles of strength m_1 and m_2 separated by a distance r is described by Coulomb's equation

$$F = \frac{\mu_0 m_1 m_2}{4\pi\mu_r r^2} \tag{1.11}$$

Where μ_0 and μ_r are the *magnetic permeability of the vacuum* and relative *magnetic permeability of the medium* separating the poles respectively.

The magnetic flux density called *magnetic field* and denoted by B, is the flux per unit area. The magnetic field B due to a pole of strength m at a distance r from the pole is defined as the forced exerted on a unit positive pole at that point.

$$B = \frac{\mu_0 m}{4\pi\mu_r r^2} \tag{1.12}$$

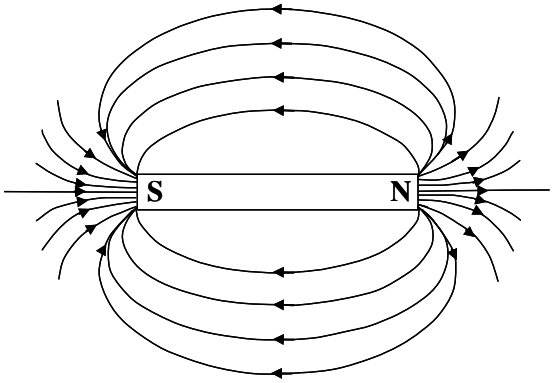

Figure 1.7 The magnetic flux surrounding a bar magnet.

Magnetic field can be defined in term of *magnetic potential* in a similar manner of gravity field. For the single pole of strength m, the magnetic potential V at a distance r from the pole is given by

$$V = \frac{\mu_0 m}{4\pi\mu_r r} \tag{1.13}$$

In the SI unit, the magnetic field B is express in Wb/m^2 = *Tesla* (T). Permeability is consequently expressed in $WbA^{-1}m^{-1}$ or Hm^{-1}. The c.g.s. unit of magnetic field strength is the *gauss* (G), numerically equivalent to 10^{-4} T (1 G=10^{-4} T).

The *Tesla* is too large to be practical in geophysical work, so the sub-unit the *nanotesla* (nT) is employed (1nT=10^{-9} T). The c.g.s. system employs numerically equivalent gamma unit (γ), equal to 10^{-15} G.

The magnetic field strength, H, is defined as the force per unit pole strength. The ratio of the flux density, B, to the magnetic field strength, H, is a constant known as *magnetic permeability,* μ. Practically, the magnetic permeability of air can be taken to be equal to the magnetic permeability of free space (a vacuum), denoted by, μ_0 of which the value is $4\pi\times10^{-7}\,WbA^{-1}m^{-1}$. For other mediums, the ratio of the permeability of a medium to that of free space is equal to the *relative permeability* μ_r, such that $\mu_r = \mu/\mu_0$. It is possible to express the relationship between B and H in term

of a geologically diagnostic parameter; namely; the *magnetic susceptibility,* κ. The magnetic susceptibility measures how susceptible material is to becoming magnetized. The magnetic susceptibility of some materials is listed in the Table 1.2. For a vacuum, $\mu_r = 1$ and $\kappa = 0$. The value of magnetic susceptibility in SI unit is 4π times value in c.g.s unit.

$$\begin{aligned} B &= \mu H \\ &= \mu_r \mu_0 H \\ &= \mu_0 H + \mu_0 (\mu_r - 1) H \\ &= \mu_0 H + \mu_0 \kappa H = \mu_0 (H + j) \end{aligned}$$

Hence $$B = \mu_0 (\kappa + 1) H \tag{1.14}$$

Since we input $\kappa = \mu_r - 1$, then $\mu_r = \kappa + 1$. From equation (1.14) we can see that in other mediums under consideration, an extra magnetizing field strength κH, called the *intensity of magnetization* or j that is induced by the H

$$j = \kappa H \tag{1.15}$$

Since κ is a dimensionless, j is also measured in Am^{-1}.

Common magnets exhibit a pair of poles defined as dipoles. The *magnetic moment* M of a dipole with pole strength of m and a distance spacing of L is given by

$$M = mL \tag{1.16}$$

Furthermore, if a volume body, V, is magnetic uniformly with intensity j, (Figure 1.8) then that body said to become a magnetic moment M which is defined as the product of magnetic pole strength m and the separating distance L, can be determined from

$$j = \frac{M}{LA} = \frac{m}{A} \tag{1.17}$$

Where A is the cross-section area of the bar magnet.

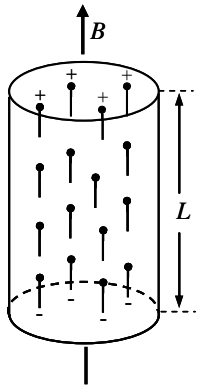

Figure 1.8 Schematic representation of an element of material in which elementary dipoles align in the direction of an external field B to produce an overall induced magnetization (Modified from Kearly et al., 2002).

Table 1.2 Magnetic susceptibilities of rocks and materials. (Hunt et al., 1995.)

Materials /Rocks	Volume magnetic susceptibility ($\kappa \times 10^{-6}$ SI)
Basalt	250-180,000
Granite	0-50,000
Clay	170-250
Coal	50
Sandstones	10-20,900
Limestone	2-25,000
Shale	5-30
Red sediment	10-100
Slate	0-38,000
Iron	3,900,000
Hematite ($\alpha - Fe_2O_3$)	500-40,000
Magnetite (Fe_3O_4)	1,000,000-57,000,000

There are two types of magnetization in an element. One attained from induction by the earth's magnetic field denoted by j_i and another is remanent magnetization denoted by j_r. The intensity of magnetization depends primarily upon the magnetic susceptibility as well as the magnetization force, and the remanent intensity depends upon the history of the rock forming, for example heating and reheating in the earth field, chemical change and so on.

Nature of magnetized material is general complex and is related to atomic properties. There are three types of magnetic materials; diamagnetic, paramagnetic, and ferromagnetic.

(1) Diamagnetism; this form of magnetism is caused by an alignment of magnetic moments associated with orbital electrons in the presence of an external magnetic field. Those elements are no unpaired electron in their outer electron shells. The magnetic susceptibility of diamagnetic material is small and negative. Quartz, feldspar, salt and halite are example of diamagnetic materials.

(2) Paramagnetism; this form of magnetism associated with elements that have an odd number of electrons in their outer electron shells. The paramagnetic associated with the alignment of the electron spin directions in the presence of an external magnetic field. It can only be observed at relatively low temperature. The temperature above which paramagnetism is no longer observed is called the *Curie temperature*. The susceptibility of paramagnetic material is small and positive. Olivine, pyroxene, biotite are example of paramagnetic materials.

(3) *Ferromagnetism*; this is a special case of paramagnetism in which there is almost perfect alignment of electron spin directions within large portions of the material referred to as domains. Like paramagnetism, ferromagnetism is observed only at temperature below the Curie temperature.

1.1.2.2 Geomagnetic field

Magnetic anomalies caused by magnetic objects or rock are localized effects superimpose on the normal earth magnetic field called geomagnetic field. The

geomagnetic field exhibits irregular variation in both direction and magnitude with latitude, longitude, altitude and time.

At any point on the earth's surface a free suspended magnetic needle will assume a position in space in the direction of geomagnetic field. The geomagnetic field can be described in term of geomagnetic elements (Fig 1.9(a)). The *total field vector* B has a vertical component Z and a horizontal component H in the direction of magnetic north. The dip of B is the *inclination* I of the field and the angle between H and geographic north is the declination D of the field. B varies in strength from about 25,000 nT in equatorial region to about 70,000 nT at the poles. In the northern hemisphere the magnetic field normally dips downward towards the north and become vertical at the north magnetic pole. In the southern hemisphere the dip is generally upward towards the north. At the equatorial region the inclination is zero (Figure 1.9(b)).

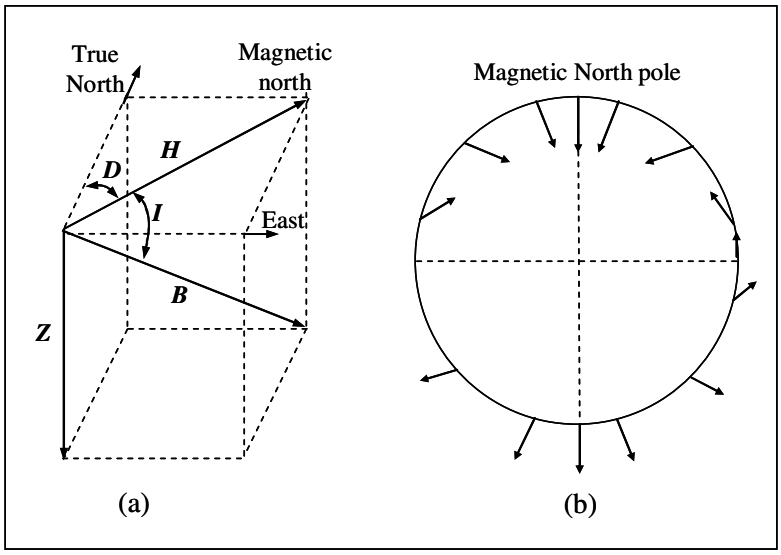

Figure 1.9 (a) Geomagnetic elements (b) variation of the inclination of the total magnetic field with latitude based on simple dipole approximation of geomagnetic field (Modified form Kearly et al., 2002).

1.1.2.3 Noise and corrections

All magnetic data sets contain elements of noise and require some form of correction on raw data to remove all contributions to the observed magnetic field other than those caused by magnetic sources. In ground magnetic surveys, any magnetic objects such as keys, penknives, some wrist-watches, etc, which may cause magnetic noise, must be kept, away from the sensor. Moreover, it is essential to keep the sensors away from magnetic objects such as cars, metal sherds, power line, metal pipe, etc.

Diurnal variation correction: Magnetic effects of an external origin cause the geomagnetic field to vary on daily basis to produce diurnal variation. Under the normal conditions (quiet days) the diurnal variation is smooth and regular and has amplitude of about 20-80 nT. Such variations result from the magnetic field induced by the flow of charge particles within ionosphere toward to the magnetic poles circular patterns. Diurnal variations vary in sympathy with the tidal effects of the sun and moon. Some disturbed days are distinguished by far less regular diurnal variation and involve large, shorterm disturbances in geomagnetic field, with amplitudes of up to 1,000 nT, known as Magnetic storms. Such days are usually associated with intense solar activity and result from solar charged particles in ionosphere. There are several ways to remove the effects of diurnal variations. For smaller scale engineering-type applications, the use of a base (reference) station near the survey area is usually deployed. This base station can either be re-occupied at a fixed time interval throughout the survey or (if possible) an instrument can record the geomagnetic field continuously at this location. The diurnal variation of the geomagnetic field can thus be subtracted from the measurements obtained in the survey area.

Geomagnetic correction: It is necessary because the Earth's magnetic field naturally varies as one move from the poles to the equator. This variation is some degree predicable and known and therefore called the geomagnetic reference field. The International Geomagnetic Reference Field (IGRF) defines the theoretical undisturbed magnetic field at any point on the Earth's surface.

Elevation and Terrain Corrections: The vertical gradient of the geomagnetic field is only some 0.03 nT /m at the poles and -0.015 nT /m at the equator,

so an elevation correction is rarely applied. The influence of topography can be significant in ground or near ocean bottom surveys, but it is not, in general, clear as to how to apply a terrain correction.

1.1.2.4 Magnetic anomaly

All magnetic anomalies caused by rock or magnetic objects depend on the geomagnetic field that is complex as the geomagnetic field varies not only in amplitude, but also in direction. Figure 1.10 shows the field of a homogenously spherical body magnetized by induction in the earth magnetic field.

The normal geomagnetic field is described by a vector diagram (Figure 1.9). The relationships of geomagnetic elements are as follows,

$$B^2 = H^2 + Z^2 \tag{1.17}$$

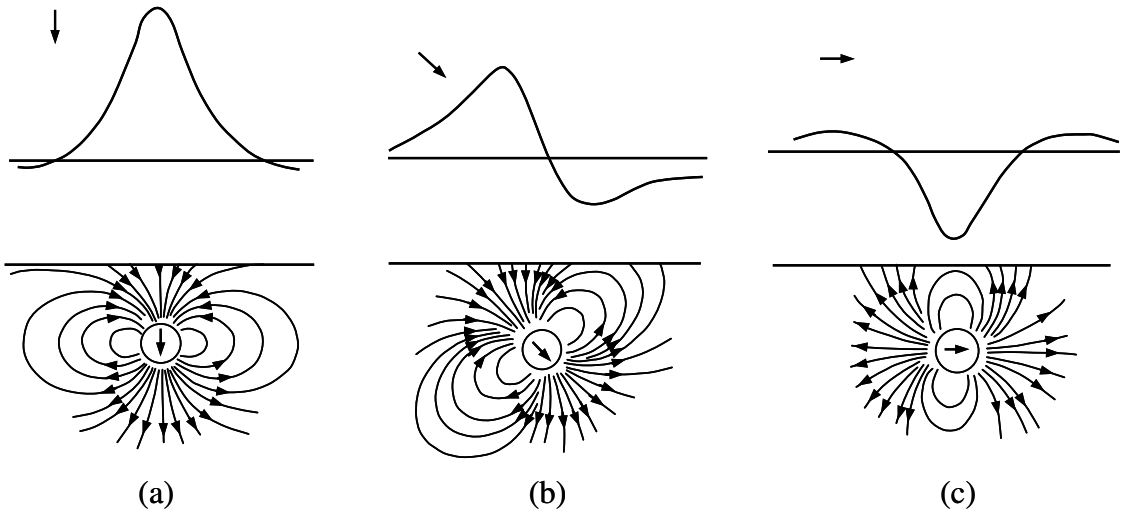

Figure 1.10 Total field anomalies for the dipole for geomagnetic inclinations (a) 90^{o}, (b) 45^{o}, and (c) 0^{o} (Modified from Griffiths and King, 1981).

Descriptions of geomagnetic element ratios is given as

$$\Delta B = \Delta Z \sin I + \Delta H \cos I \cos\alpha \tag{1.18}$$

Where α is the angle between magnetic north and the profile direction.

The magnetic anomaly of a small isolate magnetic pole strength m defined as the effect of this pole on a unit positive pole at the observation point. The pole is situated at depth z, horizontal distance x and radial distance r from the observation point (Figure 2.10). The force repulsion ΔB_r on the unit positive pole in the direction r is given by substitution in equation (1.19), with $\mu_r = 1$,

$$\Delta B_r = \frac{Cm}{r^2} \tag{1.19}$$

Where $C = \frac{\mu_0}{4\pi}$

If it is assumed that the profile lines is the direction of magnetic north so that the horizontal component of the anomaly lines in this direction, the horizontal (ΔH) and the vertical (ΔZ) components of this force can be calculated by

$$\Delta H = \frac{Cm}{r^2}\cos\theta = \frac{Cmx}{r^3} \tag{1.20}$$

$$\Delta Z = -\frac{Cm}{r^2}\sin\theta = -\frac{Cmz}{r^3} \tag{1.21}$$

The vertical field anomaly is negative because the z-axis is positive downwards. These anomalies are shown in Figure 1.11. The Horizontal field anomaly is a positive/negative couplet and the vertical is centered over the pole. The total anomaly ΔB is obtained by substituting the expression of equations (1.20) and (1.21) in equations (1.18).

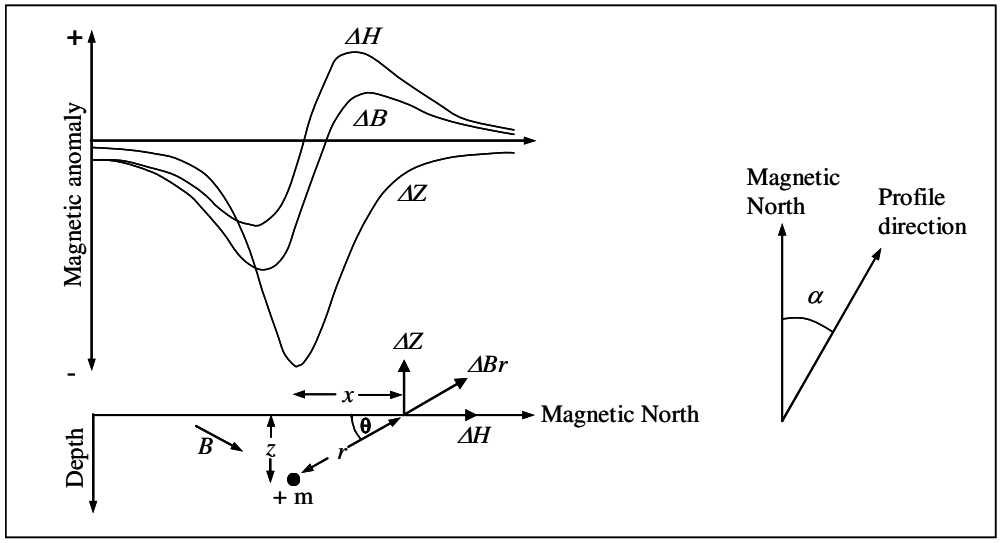

Figure 1.11 The horizontal (ΔH), vertical (ΔZ) and total field (ΔB) anomaly due to an isolated positive pole (Modified from Kearey et al., 2002).

. **1.1.2.5 Magnetic surveying instruments**

Since the early 1900s a variety of surveying instruments have been designed for measuring the geomagnetic elements Z, H and B in order to locate mineral deposits, archaeological sites, buried treasure, etc. Most modern survey instruments, however, are designed to measure B only. The required precision is normally ± 0.1 nT which is approximately one part in 5×10^6 of the background field. There are several types of magnetometers such as *torsion balance, fluxgate, proton, alkali vapour and cryogenic (SQUID) magnetometer* (Reynolds, 1997). The proton magnetometer is carried out for this project and it will be explained as follow.

The proton magnetometer, an instrument used for measuring the strength of a total magnetic field, has a sensor which comprises bottle filled in with liquid rich in hydrogen atoms such as usually water or kerosene, surrounded by a coil (Figure 1.12(a)). The hydrogen nuclei (protons) act as small dipole and normally align parallel to the ambient geomagnetic field B_e (Figure 1.12(b)). The proton precession magnetometer operates on the principal that protons in all atoms are spinning about an axis aligned with

the magnetic field. Ordinarily, protons tend to align in the earth's magnetic field. When a current is passed through the coil to generate magnetic field B_p 50-100 times larger than the geomagnetic field, and in a different direction, generated by passing a current through the coil, causes the protons to align in this new direction (Figure 1.12(c)). When the current to the coil is then switched off the polarizing fields is rapidly removed. The protons return to original alignment with B_e by or precessing around this direction (Figure 1.12(d)) with period of about 0.5 ms, taking some 1-3 s to achieve their original orientation. The frequency at which the protons precess is directly proportional to the strength of the earth's magnetic field, given by

$$f = \frac{\gamma_p B_e}{2\pi} \tag{1.22}$$

Where γ_p is the gyromagnetic ratio of the proton, an accurately known constant. Consequently, measurement of f at about 2 kHz provides a very accurate measurement of the geomagnetic field.

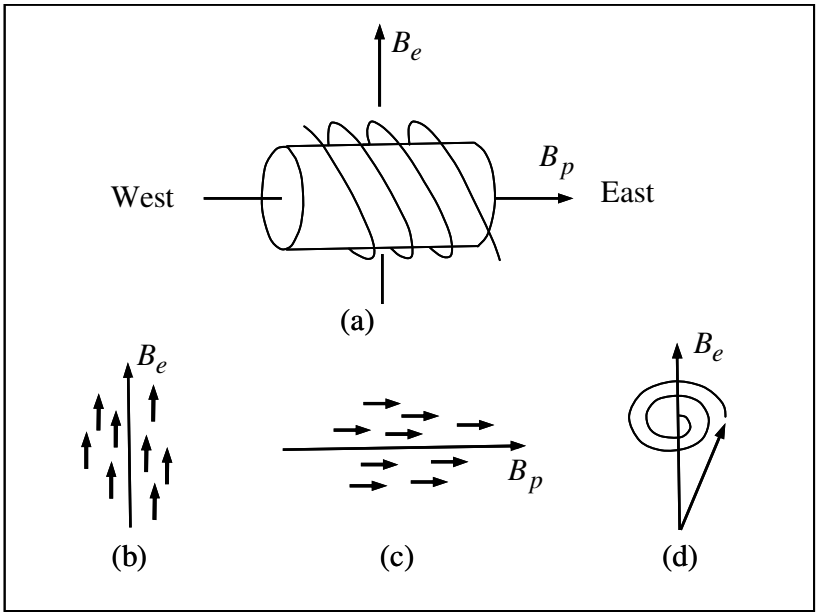

Figure 1.12 Principle of the proton magnetometer (Modified from Kearey et al., 2002).

1.1.3 Resistivity methods

Resistivity methods have been used in many applications with an aim to characterize subsurface features. In case of archaeological studies, we detect zones of anomalous in soil, which might be related to buried archaeological objects in subsurface to determine location and feature of the objects.

The electric current I is flowing through a cylindrical shaped conductor of unit cross section is governed by Ohm's law

$$I = -\frac{dV}{R} \tag{1.23}$$

Where dV is the potential difference between both ends of the conductor and R is the resistance of the conductor. The minus sign expresses the fact that the direction of current flow opposite to increasing direction of potentials. R is directly proportional to the length dL of conductor and inversely to the cross section area S. Resistivity of the material can be defined by

$$\rho = R\frac{S}{dL} \tag{1.24}$$

Where ρ is the resistivity of the conductor.

The basis of electrical resistivity measurement is to inject a known electric current into the ground and measure potential difference on the surface. The resistivity of the ground is proportional to a ratio of the measured potential difference over the injected current.

Assume that the current electrode C_1 is placed on a homogenous ground of resistivity, ρ. The current in the ground flows radially out through a hemisphere of radius r and surface area $2\pi r^2$ around the electrode (Figure 1.13). If the current, I is injected into the ground, the potential difference dV across the shell can be written by

$$dV = -\frac{I\rho\, dr}{2\pi r^2} \tag{1.25}$$

According to Ohm's law can be written in the form

$$E = \rho\, j_r = -\rho \frac{I}{2\pi r^2} \tag{1.26}$$

The potential V at a distance r from a current electrode is obtained by integral of $E_r\, dr$ from infinity to r. Assuming the potential at infinity is zero.

$$V = -\int_{\infty}^{r} E_r dr = \frac{I\rho}{2\pi r} \tag{1.27}$$

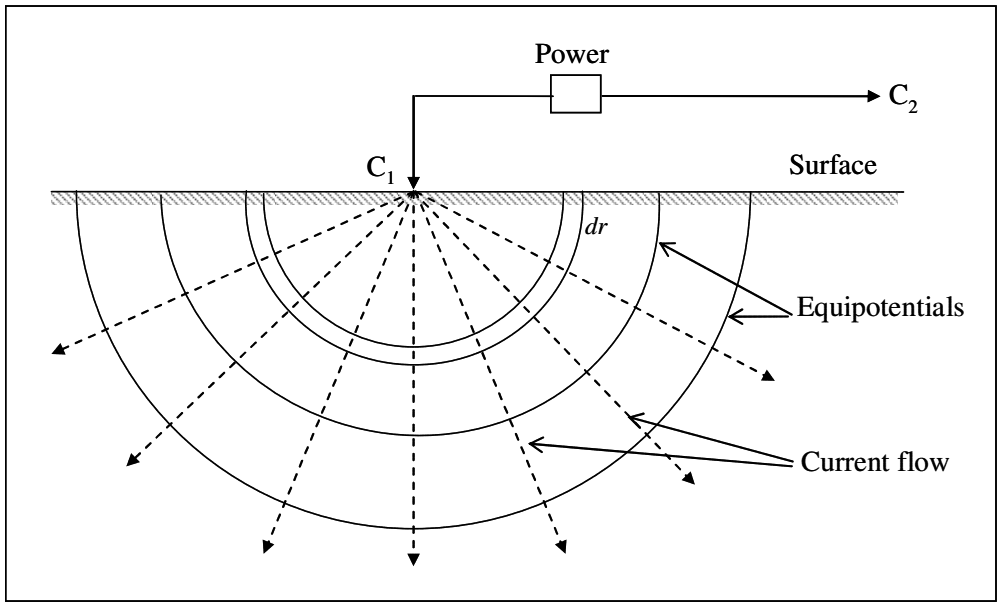

Figure 1.13 Point source current at the surface of homogenous medium (Modified from Telford et al., 1990)

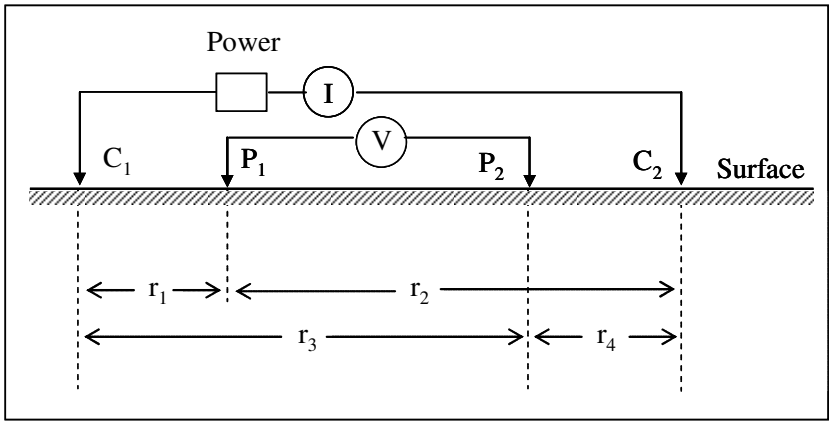

Figure 1.14 Two current and two potential electrodes array for resistivity measurement (Modified from Telford, 1990)

The electric potential at P_1 and P_2 are the following;

$$V_{P1} = \frac{\rho I}{2\pi}\left(\frac{1}{r_1} - \frac{1}{r_2}\right) \tag{1.28}$$

and

$$V_{P2} = \frac{\rho I}{2\pi}\left(\frac{1}{r_3} - \frac{1}{r_4}\right) \tag{1.29}$$

The potential difference between potential electrodes is

$$\Delta V = V_{P2} - V_{P1} = \frac{\rho I}{2\pi}\left\{\left(\frac{1}{r_1} - \frac{1}{r_2}\right) - \left(\frac{1}{r_3} - \frac{1}{r_4}\right)\right\} \tag{1.30}$$

or

$$\rho = \frac{\Delta V}{I} G \tag{1.31}$$

$$G = \frac{2\pi}{\left(\frac{1}{r_1} - \frac{1}{r_2}\right) - \left(\frac{1}{r_3} - \frac{1}{r_4}\right)} \tag{1.32}$$

G is the geometric factor depending upon the arrangement of the four electrodes.

Where the ground is homogeneous and isotopic, the resistivity of the ground is constant for any current and electrode arrangement. In contrast, if the ground is inhomogeneous, the resistivity of the ground will vary with electrode spacing. This measured resistivity is called "*apparent resistivity",* ρ_a.

The apparent resistivity will be closed to the true resistivity for short electrode spacing. The apparent resistivity is not defined an average value and it is equal to the true resistivity in case of homogenous ground. In particular, the apparent resistivity can be expressed as a function of resistance, R and the geometrical factor, G.

$$\rho = RG \tag{1.33}$$

Where $$R = \frac{\Delta V}{I}$$

In present study, there are two technique resistivity measurements. One is vertical electrical sounding (VES) for detecting one variation of electrical conductivity of the ground in vertical direction. The second is electrical mapping which determine the lateral variation in the conductivity of the ground. When the electrode spacing is fixed, the apparent resistivity depends on the electrical properties of the ground down to some depths depended on the spacing. Mapping is useful for detecting local, relatively shallow inhomogeneities and is employed typically in ore prospecting and in delineating geologic boundaries, fractures, cavities. It has also been used in archaeology for locating ancient buried structure. Pseudosections, vertical and horizontal variation resistivity can be obtained at once by combined VES and mapping called CVES.

In continuous vertical electrical sounding (CVES), the common arrays that employed for two dimension (2-D) resistivity imaging are Wenner, dipole-dipole, Wenner-shlumberger, pole-pole and pole-dipole. The best chosen array depends on types of the structures to be mapped, sensitive of equipment of the resistivity and manpower.

The apparent resistivity of ground measured with different can be calculated in follows;

Wenner array: $$\rho_a = 2\pi a R \tag{1.34}$$

Dipole-dipole array: $$\rho_a = \pi n(n+1)(n+2)a R \tag{1.35}$$

Electrode array for Wenner mapping of which shown in Figure 1.15(a) with the spacing between electrodes, a is fixed during the measurement, and all electrodes are moved together along the line.

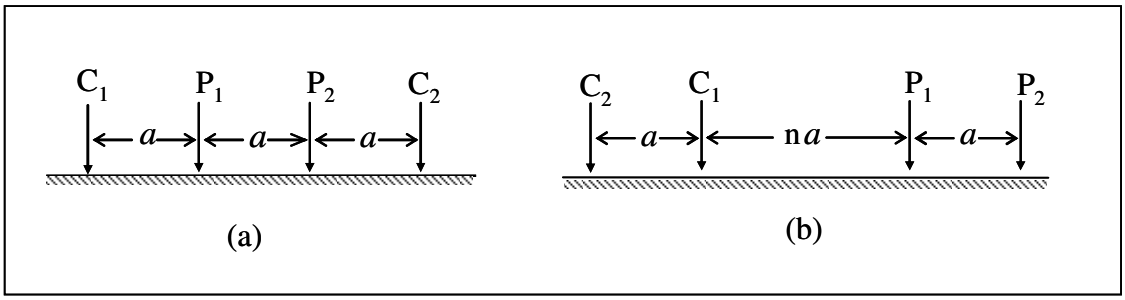

Figure 1.15 Common electrode arrays used in resistivity survey; (a) Wenner array and (b) dipole-dipole array.

An increase of a will increate depth of investigation. Hence the resistivity pseudosection can be obtained when the electrode spacing is increased and move along the same line like the first step and so on until the depths of investigation are reached. Continuous vertical electrical sounding (CVES) with dipole-dipole array is shown in Figure 1.15(b). Electrode array is moved as a whole along measuring line by fixing the value of a and varying values of n. In displaying the result, lines making an angle of 45^{o} with horizontal line are drawn from the center of current and potential dipole in opposite direction values of apparent resistivity are plotted at intersection of there two lines (Figure 1.16). When n increases, the plotting point will be at deeper location. The pseudosection can be constructed when the current dipole are moved toward at a step of a to complete a measuring line.

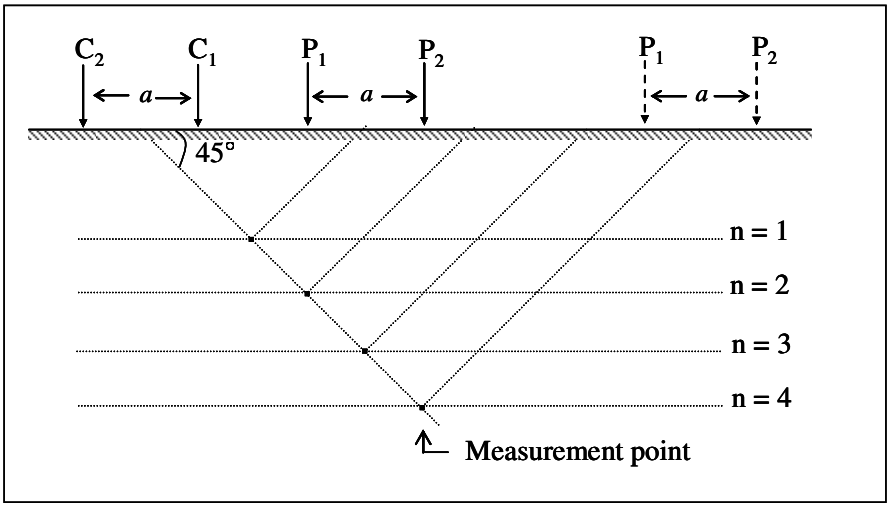

Figure 1.16 CVES plotting with dipole-dipole array (Modified from Parasnis, 1997).

In general pore in rocks are filled by water. The resistivity of porous, water-bearing rock is determined by Archie's empirical equation.

$$\rho = a\,\rho_w\,\Phi^{-m} s^{-n} \tag{1.36}$$

Where ρ_w is the resistivity of the water filling in the pores, Φ is the porosity (volume fraction of pore), s is the volume fraction of pore filled with water, and a, m and n are empirical parameters. The value of m depends on the degree of cementation ($1.3 \le m \le 2.5$). The value of n is nearly 2.0 if more than 30% of pore is water-filled. However, the value of n can be much greater for lesser water contains. The value of a is $0.5 \le a \le 2.5$. The resistivity of geologic materials is shown as Table 1.3.

Table 1.3 Resistivities of common geologic materials (Reynolds, 1997)

Material	Nominal resistivity (Ωm)
Soil (with 40% of clay)	8
Soil (with 20% of clay)	33
Top soil	250-1700
Laterite	800-1500
Laterite soil	120-750
Alluvium and sand	10-800
Dry sandy soil	80-1050
Sandy clay/ clayey sand	30-215
Rainfall runoff	20-100

1.2 Literature review

1.2.1 Detail of study area

Lao Pako located in Phonekham village. Lao Pako is associated with Nam Ngum River, one of the largest tributaries of the Mekong River that flows from Xiang Khaung province, northern Laos and through the Lao Pako landscape. Lao Pako locates on a small hill at southern bank of the Nam Ngum, at the sharp bend of the coast of the river both upstream and downstream. Its elevation is about 170 m above sea level.

Lao Pako, in Lao, means literally a young forest of *ko* trees: *Lao pa* is young forest, and *ko* is a name of tree that grows in abundance in the area. For along, Lao Pako was known among people nearby the villages as a *phi pa sa*, a place where spirits are. Presently, Lao Pako is known as Ban Pako eco-tourist resort. Lao Pako was become an archaeological site in the early 1990s, when the established resort on the site was found archaeological materials were unearthed during construction period of the resort. The first excavation, a trench was conducted in 1994. For the archaeological investigation

is required for Lao Pako in order to gain a better understanding on history of the site and origin of archaeological evidences.

In 1995, the first excavation under joining between Lao and Swedish archeologists was conducted. The aims of excavation were to find out what kind of artifacts remain in the site, how old they were, and to identify what kind of contexts they belong. Three trenches with various sizes were excavated cover areas of 25 m^2. The excavation revealed large quantity of artifacts, potteries, and iron production materials. So this evidence shows that Lao Pako was a place for rituals, involving pottery deposition and small-scale iron production between approximately 350 and 600 AD (Källén & Kralström, 1999).

In 2000, Anna Källén, a Swedish archaeologist, and the Ministry of Information and Culture (MIC) continued their work with the Lao Pako. There were three objectives in the investigation. The first one was need to put Lao Pako in a physical context. Secondly, to test whether archaeological theory such as a field kit phosphate analysis (Perssion, 1997). Thirdly, to have involved local community involved in previous excavation and to gain their knowledge on physical and cultural setting of the site. The survey areas covered area of about 20 km^2 including Ban Nabong, Ban Phonekam, and Ban Tha Kok Hai. The investigation results showed more than twenty archaeological sites previously unknown to authorities were identified and one of there is roughly contemporary with Lao Pako site whereas the rests are in recent time. The phosphate mapping with a 10 x 10 meter grid in Lao Pako and a few locations in vicinity grave found clear pattern of quite remarkable phosphate concentration at the top of the hill where the tourist resort is today (Källén & Karlström, 1999; Karlström and Källén, 2000; Bousisengpaseuth et al., 2000).

In 2002-2003, the excavation was conducted in order to gain understanding of the distribution and composition of the cultural materials over the areas where high concentration of phosphates was observed. All together 3 trenches and 16 test pits, had been excavated, covering area of 41 m^2 which is approximately 6.4% of the total study area. The artifacts were grouped into five categories: *Ceramics, Textile Production, Breads, Metal and Metallurgy, and Stone* with following details;

Ceramics: The ceramic from the three excavation period of 1995, 2000 and 2002-03 has been analyzed into two groups: complete vessels and sherds shown in Figure 1.17. The total of 76 ceramic complete vessels, deposited in pits, have been recovered and reconstructed. The total 5,175 potsherds with the total weight of 47 kg are founded secreted on the former ground surface and in the pits. These have stored at Laos National Museum in Vientiane.

Textile Production: There are two categories of artifacts that associate with textile production found in Lao Pako: spindle whorls and clay seals (Figure 1.18). A total number of 44 spindle whorls were recovered, of which 30 were found in the cultural layers. The spindle whorls are made of fired tempered clay. Some of these are good condition, while others are deteriorated and appear to be almost dissolved by the soil moisture. Similarly 4 clay seals with different shapes were found in the cultural layers and in the same areas where spindle whorls appear.

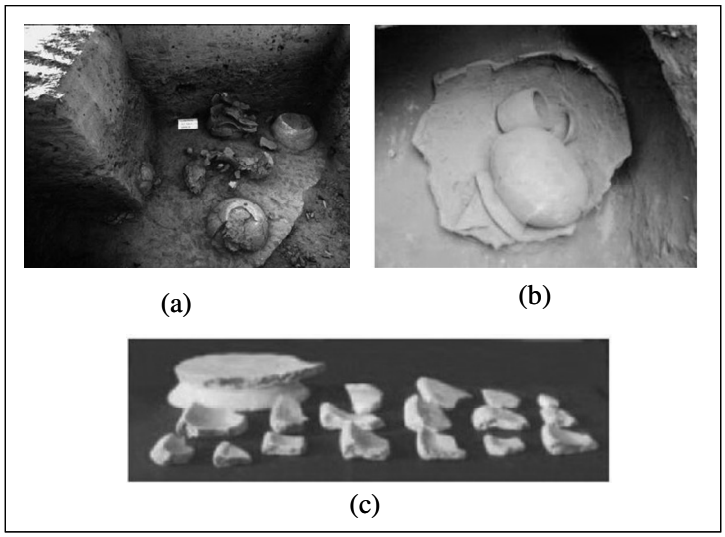

Figure 1.17 Excavation in 2003 (a) a pit with vessels and potsherds, (b) potteries, and (c) potsherds with different shapes (Källén, 2004).

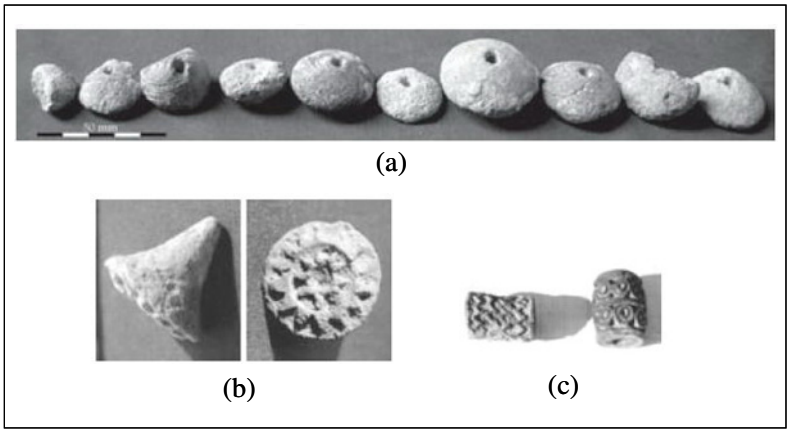

Figure 1.18 Excavation in 2003 (a) ten spindle whorls, (b) clay seal, diameter 30 mm, and (c) stamp roller (Källén, 2004).

Breads: all beads made of glass that varies in size, shape and color, translucent and opaque. But one is made of cornelian: large spherical, semi-translucent and amber colored (Figure 1.19). A total number of 346 beads have been found in Lao Pako, in 17 discrete contexts.

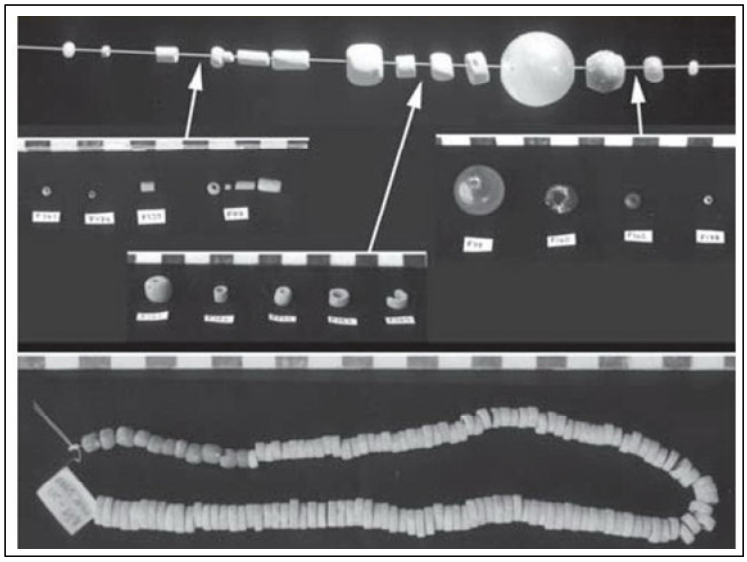

Figure 1.19 Glass beads from the 2003 excavation (Källén, 2004).

Metal and Metallurgy: Lao Pako was a metal production site (Källén & Kralström, 1999). There are found large amount of bowl shaped iron slag, tuyères, dross on pebbles and pottery vessels, scattered iron objects, and fired clay, were found. There are large amount of iron slag exposed on the ground southeastern slope of the hill. Broken tuyères were found at the same level where there are iron object scattered around. The tuyères are made of clay with wider opening one end and rounded one, often covered in metallic substances. It is probably loading into the hearth or furnace (Figure 1.20(b)). Because, there is no evidence of furnace, but only some remains of fired clay appear to be some sort of minor structures. It probably indicates that the Lao Pako iron product ion was performed in small scale and only with forging of smelted bloom. The metal objects found at Lao Pako are either bronze and iron (Figures 1.20 and 1.21). Iron objects mostly found in cultural layers.

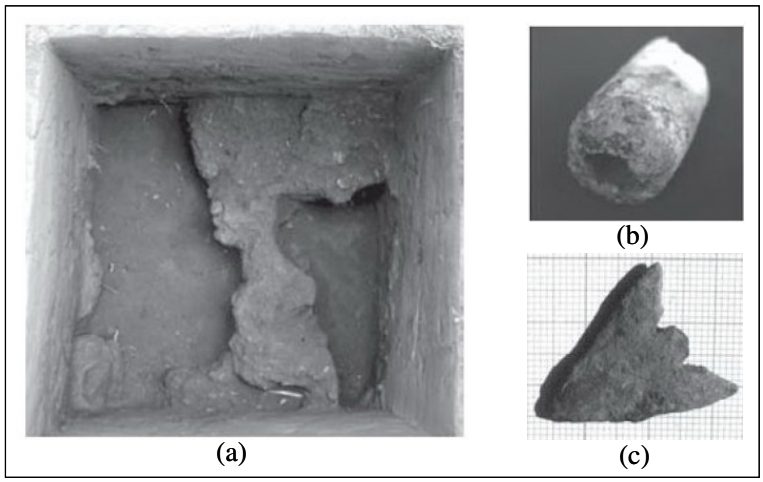

Figure 1.20 Objects relating to iron working (a) structure of fired clay, (b) tuyères, and (c) iron narrow head (Källén, 2004).

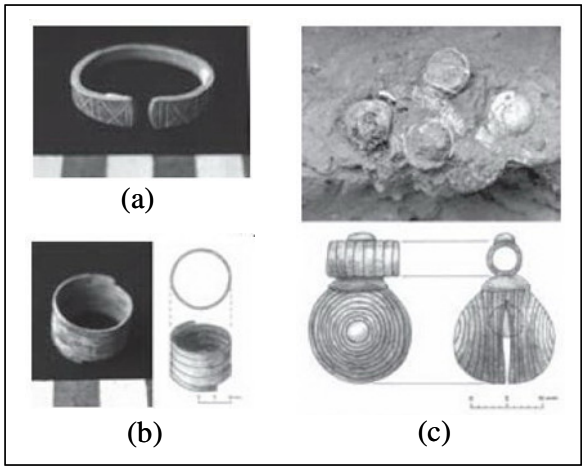

Figure 1.21 Objects relating to iron working (a) bronze bangle, (b) bronze helix ring (c) bronze bells (Källén, 2004).

Stone: a great variety of stone objects and artifacts have been found at Lao Pako. The largest group consists of pebbles of varying size and quality. Another category is whetstones made of fine sandstone (Figure 1.22(a)). A total number of five stone adzes were found in the excavation (Figure 1.22(b)). Only one piece of jewelry was found fragmentary stone bangle made of polished stone.

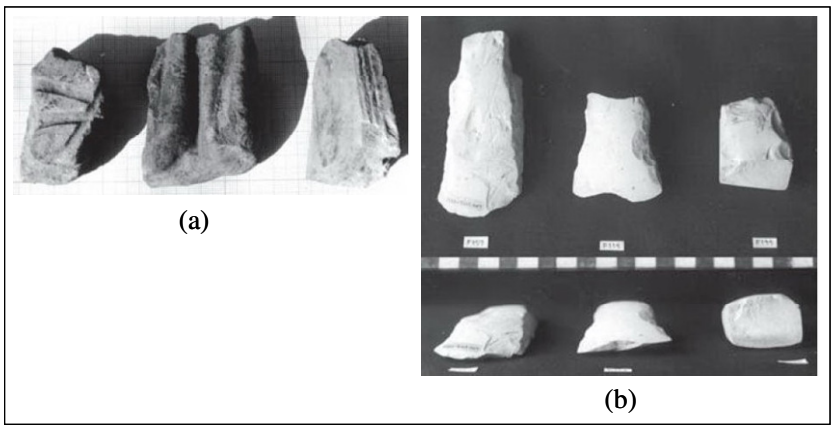

Figure 1.22 Stone objects (a) whetstones, (b) stone adzes (Källén, 2004).

Lao Pako soil was categorized into three layers as shown in Figure 1.23 (Källén, 2004). They are top soil, cultural layer and sterile soil. The top soil is fine silt without natural inclusions of gravel or larger stones. It is well sort and homogenous in color. In general, layer of topsoil varies in thickness between a few decimeters and up to a meter. Almost, no cultural material contains in this layer, however it is disturbed by termite nets. Beneath the topsoil is cultural layer, which varies in thickness and complexity between different pits. Rich in cultural materials of different kinds such as potsherd, fired clay, metallurgy material, charcoal, and miscellaneous artifacts, were found in this layer. Under the cultural layer is sterile soil, which appears approximately 0.5 m deep and varies in thickness, is sandy clay with yellowish inclusion. About 1.5 to 2.0 m down begins a layer of packed concrete-like sterile interspersed with small lump of laterite, on average 30-60 mm in diameter (Källén, 2004). There is no cultural material in this layer.

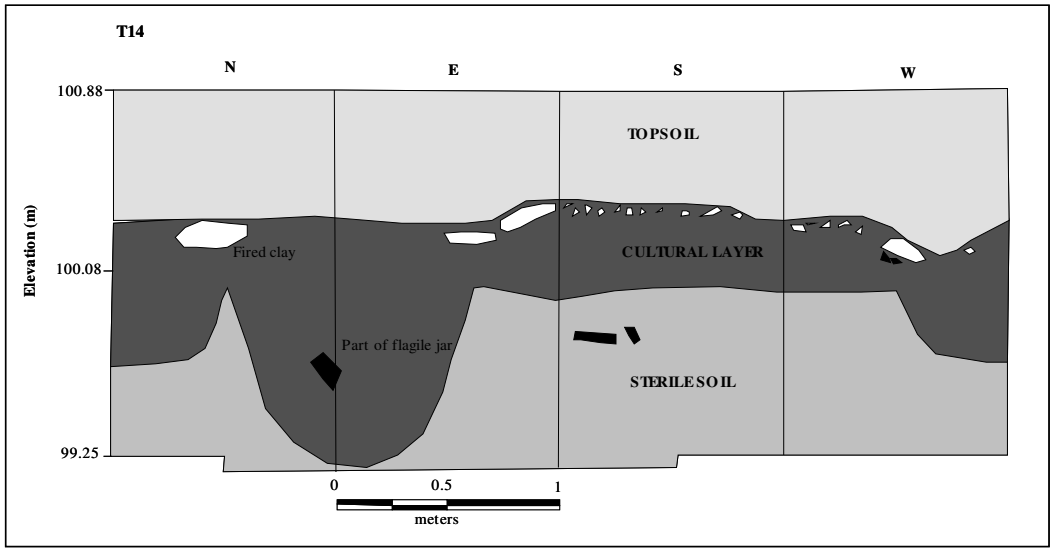

Figure 1.23 Schematic section of the archaeological stratigraphy in the study area (Modified from Källén, 2004).

1.2.2 Application of geophysical methods for archaeology

Geophysical investigation methods have been utilized widely for archaeological investigations due to their non-destructive techniques and providing high resolutions. The successes of application geophysical methods are summarized as followings;

Sambuelli et al., (1999) carried out multi-geophysical methods, magnetic, resistivity tomography and GPR methods, on a Roman archaeological site, Secondo valley (Biella, Italy) in order to map ancient walls and stone structure of 16^{th} century.

The ground penetrating radar was conducted inside the Cathedral of Valencia, Spain. The radar data were successful in locating crypts, ossuaries, sepulchers, and graves, and the location of ancient walls that existed before the final Cathedral expansion. Moreover, the result of GPR investigation was able to detect three cultural layers corresponding to the three periods of construction; Roman, Arabian and Middle Age Epochs. In addition, GPR was also used for analyzing relative moisture in the sub-areas by comparing dielectric permittivity changes and radar velocity changes between materials in humid and non-humid areas (Gracia et al., 2000).

The ground penetrating radar carried out in an urban area (Lecce, Italy) to obtain a detailed characterization of the most superficial layers, where presumably archaeological structures are buried, and to quickly identify anomalous zones for excavation. The information was obtained only between the ground level and the top of the calcarenitic basement. The analysis of the radar sections of a barrel-vault cavity was obtained from radar section analysis and subsequently confirmed by archaeological excavations (Basile et al., 2000).

Cezar et al., (2001) carried out the ground penetrating radar GPR at two archaeological sites, Serrano and Morro Grande, in Araruama County, Rio de Janeiro, Brazil, in order to aid the study of a prehistoric indigenous culture, associated with the Tupinamba tribe that inhabited the region during prehistoric times. The archaeological remains of the study area are mainly characterized by pottery artifacts for several uses, including funerary urns, buried within layers of sand and clay. A radar section acquired on an urn filled with air showed a well-marked feature.

The joint application of electric and magnetic techniques for near-surface exploration represents a very useful tool for archaeological investigation and can provide a quantitative contribution to describe the spatial distribution of buried objects in archaeological site of Pompii (southern Italy). This work showed a new advanced topographic approach, base on the parallel inversion of magnetic and electric observed data aimed to reconstruction of the subsoil of the site. The results gave information about both the position of the geophysical sources and their dimensions (Fiore et al., 2007).

The application of High Density Resistivity Method (HDRM) used for archaeological prospecting in Tenghualuo Neolithic Relict, Eastern Jiangsu, China was carry out in order to locate ash pits, rampart and moat of which density is very high (Kai et al., 2004).

Magnetic surveying was used in the Harmanoren Necropolis to locate buried grave jars before archaeological excavation. Spectral methods, horizontal plannar trend, reduction to the pole, and analytic signal were used in data processing. Horizontal plannar trends were removed from the gridded data set and then the residual anomalies were presented as contour maps. The high magnetic anomalies were interpreted as buried grave jars. After application of reduction to the pole, some form of distortion appears to remain on magnetic anomalies. Analytic signal was successfully used to determine the horizontal of buried structures causing magnetic anomalies. The advantage of the method is that its amplitude is independent on magnetization in two dimension case while in three dimension case; amplitude of the analytic signal is dependent on the body magnetization (Büyüksaraç et al., 2006).

Vafidis et al., (2005) integrated geophysical studies at ancient Itanos (Greece) in order to map buried relics of buildings, streets and walls of ancient Itanos. The integration of the geophysical measurements revealed the existence of a wall and three parallel walls verified by excavation.

Geophysical investigation of the Temple of Apollo (Hierapolis, Turkey) was carried out two geophysical methods, Ground penetrating radar (GPR) and electrical resistivity tomography (ERT) for search archaeological features (voids, walls, etc.) in subsurface. Two-dimensional ERT imaging was used to detect the presence of an active

normal fault passing under the Temple of Apollo. The resistivity profiles reveal the presence of conductive material (clay) covering the archaeological structures. In addition, three-dimensional GPR imaging was used to detect man-made structures located under the Temple of Apollo (Negri et al., 2006).

1.3 Objective

The objective of this research is to map cultural layer related with human activity in the past in the study area with combination of geophysical methods; ground penetrating radar, magnetic mapping, resistivity mapping and continuous vertical electrical sounding.